Observing Long-lived Photogenerated Holes in Cobalt Oxyhydroxide Oxygen Evolution Catalysts

Ruben Mirzoyan, Alec H. Follmer, and Ryan G. Hadt*

Division of Chemistry and Chemical Engineering, Arthur Amos Noyes Laboratory of Chemical Physics, California Institute of Technology, Pasadena, California 91125, United States

*Corresponding author: rghadt@caltech.edu

Abstract

Steady-state and time-resolved spectroelectrochemical optical absorption techniques were used to investigate photoexcited states of amorphous cobalt-phosphate oxyhydroxide (CoPi) and cobalt-borate oxyhydroxide (CoBi) oxygen evolution catalysts. These materials revealed concurrent spectroelectrochemical intensity changes in their ground state and photoexcited visible spectra, providing insights into the dynamics of defect states attributable to trapped holes. Notably, long-lived photoexcited states, assignable to hole-based defects persisting beyond 10 ms in H_2O, were observed in CoPi and CoBi for the first time. Both thin films exhibited distinct dynamics, however, highlighting differences in their structural and electronic properties despite strong similarities in absorption spectral profiles. These results provide further insight into the differences between the electronic properties and dynamics of CoPi and CoBi, which have been challenging to structurally and electronically characterize due to their amorphous nature.

1. Introduction

Materials and devices that harvest photon energy and convert H_2O into fuel in the form of H_2 provide a promising avenue to an alternative renewable energy infrastructure.[1–3] The oxygen evolution reaction (OER) is a key bottleneck to the water-splitting process, with many historically successful catalysts being comprised of expensive, non-earth-abundant metals.[4] Amorphous cobalt-phosphate oxyhydroxide (CoPi) is a self-healing oxygen-evolving catalyst with a low overpotential at neutral pH.[5,6] It has been integrated with a variety of semiconductor-based light-harvesting materials[7–14] and is a key component of the 'Artificial Leaf', a triple-junction

amorphous silicon photovoltaic with a ternary alloy and CoPi interfaced on either side for the hydrogen and oxygen evolution half-reactions, respectively.[7] This device proved to be extremely robust, operating in natural water conditions for days with no decline in activity.

Until recently, the photophysical properties of CoPi have not been considered in detail. Sprague-Klein et al. demonstrated direct photochemical effects on the OER through wavelength-dependent electrochemical responses with either 415 nm or 623 nm LED irradiation.[15] With 415 nm excitation, the overpotential increased, while the opposite effect was observed for 623 nm excitation. These effects were attributed to photoinduced redistributions of electron density within Co–O bonds, with shifts toward oxygen improving the surface oxo reactivity previously implicated in the mechanism of O–O bond formation.[6,16–19]

In addition to CoPi, electrodeposited thin films from borate buffer (CoBi) have provided comparative insights into thin film formation and stability.[20] Cyclic voltammograms of thin films in their respective buffers show Co(II)/Co(III) quasi-reversible redox features at 1.05 V vs. NHE (CoPi) and 0.88 V vs. NHE (CoBi) (**Figure 1**).[21] There also exists a Co(III)/Co(IV) redox feature near the onset of the OER catalytic wave, with Co(IV) formation representing a mechanistic prerequisite for catalysis. Interestingly, Costentin et al. have also correlated the presence of high valent Co(IV) to a semiconductor-type charge transport in the thin film. Relatedly, it was further observed that the proton-electron conductivity increases with applied anodic potential and is higher for CoBi than CoPi.[21]

These electrochemical and conductivity differences have been related to the distinct morphologies of CoPi and CoBi.[16,21,22] Co K-edge extended X-ray absorption fine structure (EXAFS) data suggested both films are comprised of edge-sharing MO_6 clusters of molecular dimensions.[19,23,24] Pair distribution function (PDF) analysis further revealed that the intermediate-range structure differs substantially between CoPi and CoBi: CoBi is more structurally coherent, resembling a layered structure similar to CoO(OH) with 3 – 4 nm clusters making up coherent domains, while CoPi consists of smaller clusters that are not coherently stacked.[22] A combination of X-ray spectroscopies and model compounds have also been used to propose that CoPi is comprised of 44% O_h Co(III), 39% O_h Co(II) and 17% T_d Co(II), while CoBi is comprised of 65% O_h Co(III) and 35% O_h Co(II).[25] The T_d Co(II) uniquely present in CoPi was proposed to exist at edge atom sites (**Figure 1**).[25] Along with the established morphological differences, the presence of distinct coordination sites may play important roles for charge transport and catalysis.

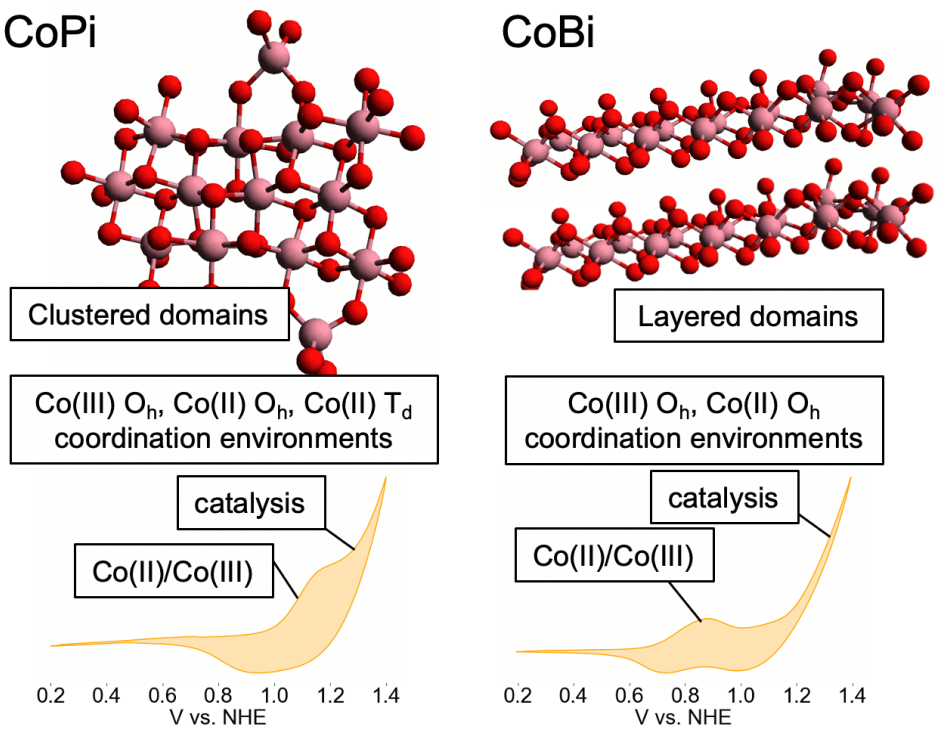

Figure 1. Graphical qualitative depictions of CoPi and CoBi domains with overview of morphological and voltametric differences under pH 7.0 and pH 9.2 buffered conditions, respectively.

To gain further fundamental insight into the structural and electronic differences between CoPi and CoBi, and to explore their photophysical properties, we carried out steady state and time-resolved optical spectroscopic studies of the two thin films. Upon 380 nm excitation, we observed, for the first time, distinct differences in photophysical behavior between the two materials, along with relaxation processes attributable to hole-based defect sites that persist beyond 10 ms. Ground- and excited-state spectroelectrochemistry further revealed insights about the band structure of CoPi and CoBi. Thus, this study provides new spectroscopic signatures that may be related to their differences in charge transport and oxygen evolution reactivity.

2. Results

2.1. Steady-state and ultrafast transient absorption spectra of CoPi and CoBi films

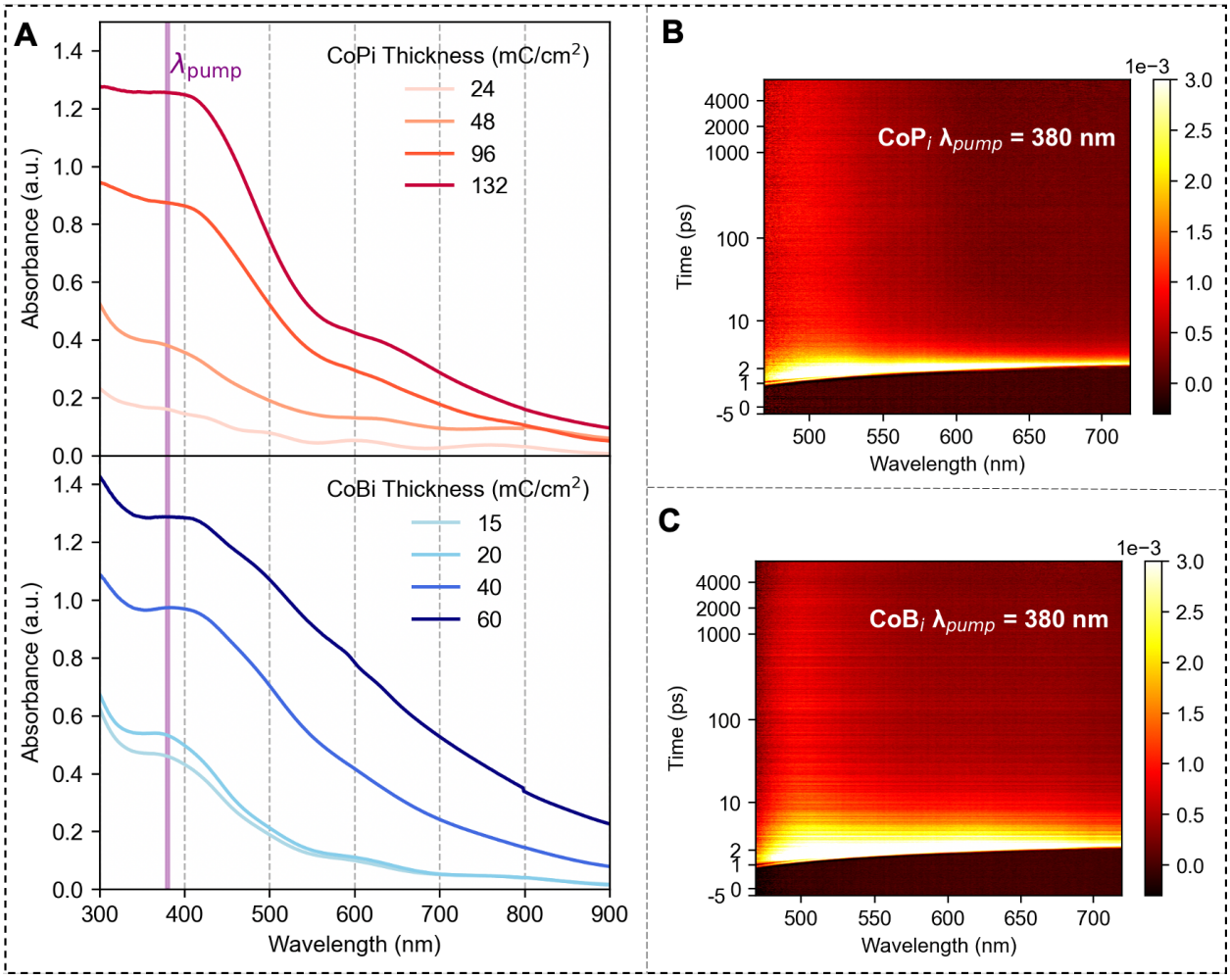

Figure 2. Steady state and time-resolved electronic absorption spectra of CoPi and CoBi thin films. (A) Background-subtracted (FTO + buffer) UV-vis absorption spectra of CoPi and CoBi films of varying thickness. Two-dimensional transient absorption spectra of 96 mC/cm^2 CoPi (B) and 48 mC/cm^2 CoBi (C) thin films collected with 380 nm pump excitation in their respective buffers.

Thin films of CoPi and CoBi electrodeposited on fluorine-doped tin oxide (FTO) both exhibit a relatively intense electronic absorption band at ~400 nm, with lower intensity absorption at wavelengths > 500 nm (**Figure 2A**), the latter of which are more intense for CoBi films. The background FTO absorption spectrum exhibits oscillations due to thin film interference (**Figure S1**). However, interference contributions are minimized with increasing CoPi/CoBi film thickness, which is proportional to the amount of charge passed during electrodeposition (mC/cm^2). Films

were between ~100 nm and ~1 μm, as determined separately through profilometry (**Table S1**). Band energies do not change with film thickness.

In addition to ground-state spectra, transient absorption measurements were carried out to probe the excited-state dynamics and to gain additional insight into the electronic structural differences between CoPi and CoBi. Optical transient absorption spectra of CoPi (**Figure 2B**) and CoBi (**Figure 2C**) in H_2O excited with a 380 nm, ~120 fs pump pulse exhibit broad excited state absorption (ESA) features that appear immediately after excitation. Power titrations ensured pump pulse energies were within the linear response regime (**Figures S5, S6**). Also, film thickness affects the overall excited-state population, but not the corresponding kinetics or spectral profiles (**Figure S13**). Spectral traces at characteristic time points reveal an ESA at ~500 nm, along with a broad, less intense ESA at ~600 – 720 nm (**Figure 3**). ESA band energies are similar between CoPi and CoBi, suggesting excited-state spectra do not reflect changes in intermediate-range structure or film morphology. While there is some variability in the relative intensity of the 600 – 720 nm region between films (**Figures S11, S12**), in all cases the ~500 nm feature blue shifts with time, while the lower energy region red shifts. The early time dynamics differ significantly between CoPi and CoBi. At time delays of 1 ns and below, the CoPi excited state signal decays much faster than CoBi (**Figure 4**, top panel).

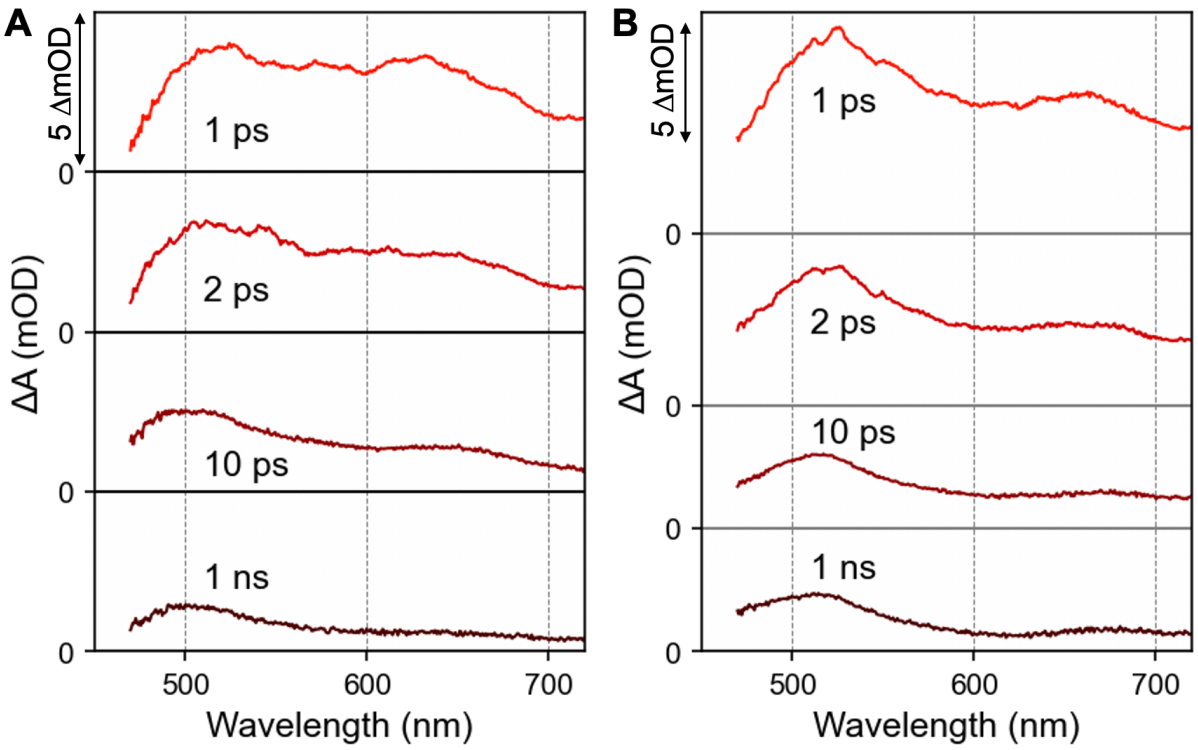

Figure 3. Spectral traces of (A) 96 mC/cm^2 CoPi and (B) 48 mC/cm^2 CoBi in H_2O at characteristic time delays.

2.2. µs and ms timescale excited state dynamics of CoPi and CoBi thin films

Using a tunable Nd:YAG laser, 380 nm pump, single wavelength probe (500 nm) measurements were used to quantify excited-state dynamics on longer, µs and ms time scales. A 10 ns pulse width excitation relative to ~120 fs (*vide supra*) increases the pulse energy by three orders of magnitude while maintaining a similar average power, allowing for the collection of weaker transient absorption signals out to significantly longer times. Indeed, ESA signals for CoPi and CoBi films in water persisted beyond 10 ms, with comparative traces for a 500 nm probe across multiple time regimes given in **Figure 4**. Despite relaxing more rapidly on the ultrafast time scale, the overall CoPi transient absorption signal decays more slowly than CoBi (**Figure 4**, middle and bottom panels). Note higher pulse powers resulted in a rapid photodissolution of the thin film, limiting the number of usable laser shots before the excited portion of the film became optically transparent (**Figure S7**). Despite this, there were no apparent changes in decay kinetics as the films dissolved upon irradiation. Nevertheless, the thickness of the film was not conserved over the course of a measurement. It was further shown that this long-lived ESA is not due to heating, as temperature-

dependent steady state absorption spectra give rise to a distinct difference signal relative to the observed ESA (**Figure S10**).

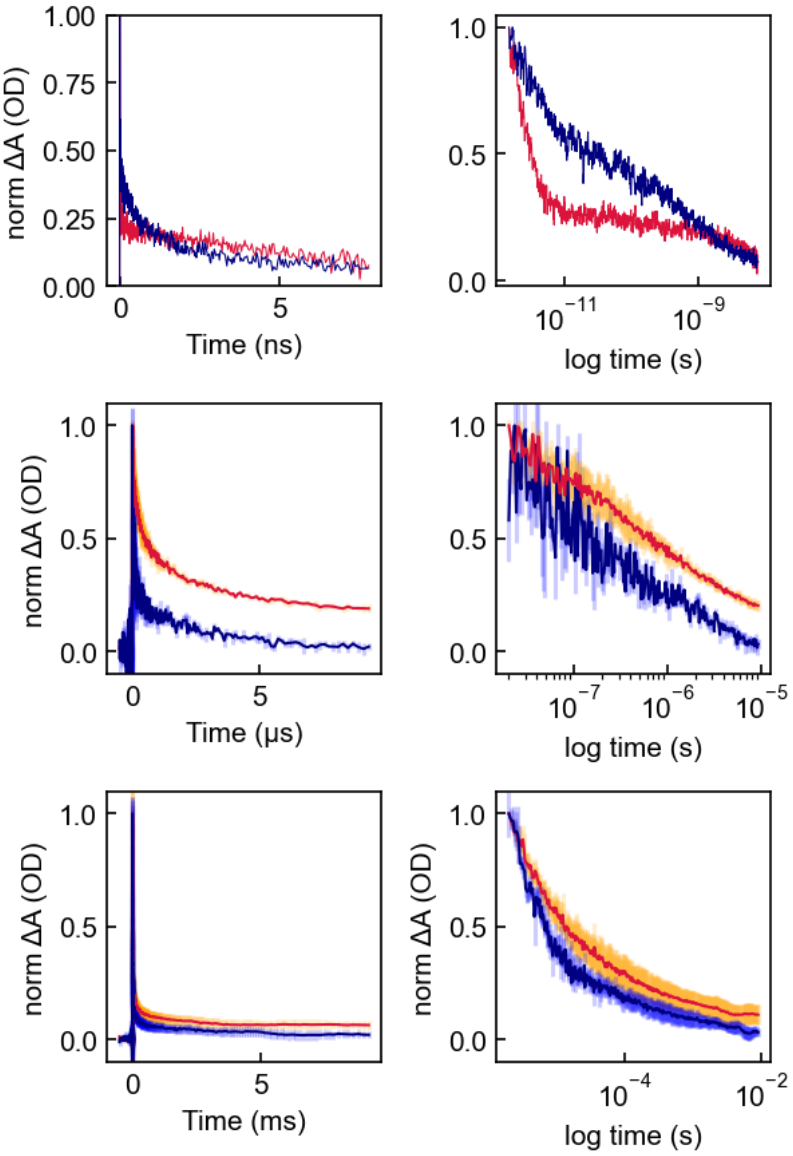

Figure 4. Comparative decay traces (380 nm pump, 500 nm probe) of CoPi (red) and CoBi (blue) in H_2O spanning nearly 10 orders of magnitude of time decay from sub-ps to 10 ms. Top row: 7 ns range decay with an ~120 fs pulse width ultrafast laser. Second and third rows correspond to time ranges of 10 μs and 10 ms, respectively, with a 10 ns pulse width Nd:YAG laser. Traces correspond to the average normalized decay of multiple films; error bars correspond to the standard deviation.

The long-lived excited-state decay was investigated in the presence of various solvents to determine whether hydrogen bonding, polarity, and/or electron/hole scavenging influenced the dynamics. Only MeOH, a hole scavenger, had a substantial effect (**Figure S32**). Averaged decay

curves obtained for both CoPi and CoBi in H_2O vs MeOH probed at 500 nm are shown in **Figure 5**, while individual constituent decay curves are shown in **Figures S23 – S29**.

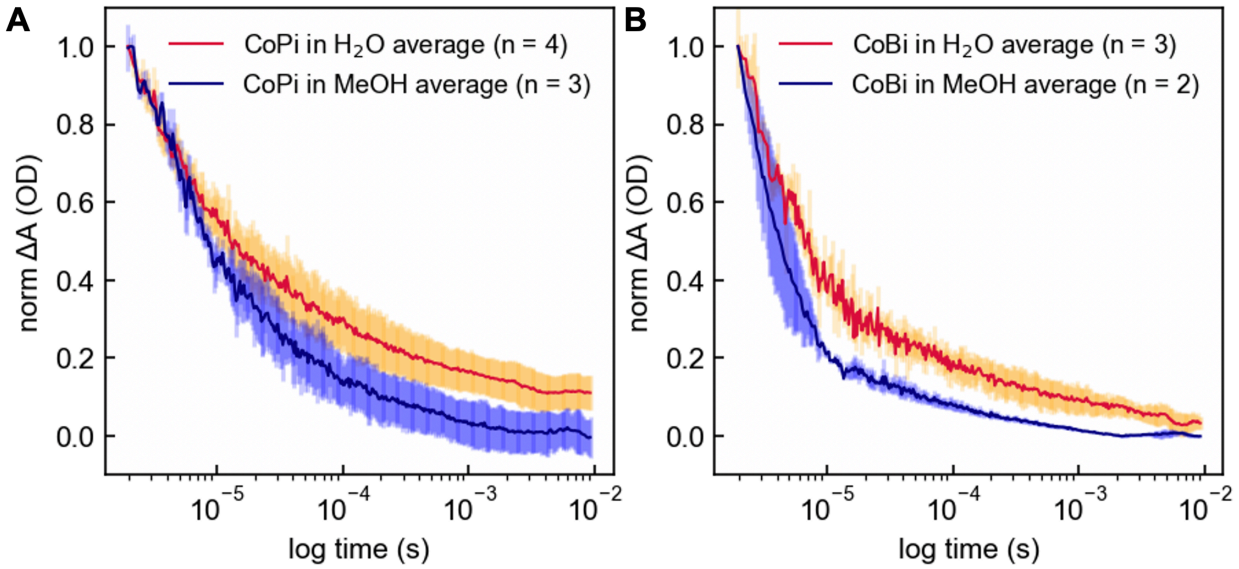

Figure 5. Comparison between the excited-state decay of (A) CoPi films immersed in neat H_2O vs MeOH and (B) CoBi films immersed in neat H_2O vs MeOH. Error bars represent standard deviations.

2.3. Spectroelectrochemistry in the ground- and photo-excited states

Distinct steady state and time-resolved spectral changes are observed for CoPi and CoBi thin films upon application of an electrochemical potential (**Figure 6**). When the potential is scanned anodically from the open circuit potential (OCP), the ground-state absorption intensity increases over the whole spectral range for both CoPi and CoBi (**Figures 6A** and **6B**, respectively). This spectral intensity change is reversible to a certain extent for both thin films when a reducing potential is applied to the oxidized films. Without actively reducing the films, they remain at a more oxidized state, possibly due to an electrochemically induced phase transition. The increase in visible absorption is evident even upon visual inspection of two films, one of which has been held under anodic bias (**Figure S17**). Note there is some variability in the shapes of the difference spectra (**Figures S18, S19**). However, the general observation is that for both CoPi and CoBi films, the change in spectral intensity is nearly uniform across the UV-vis region, with greater change occurring in the UV region.

To compare ground-state spectroelectrochemical changes to dynamics in the excited state, we further carried out spectroelectrochemical optical transient absorption spectroscopy (**Figure**

5C, 5D). In contrast to the increase in ground state absorption intensity with anodic bias, the ESA intensity decreased with anodic bias for all time delays up to 7 ns (**Figures S19, S20**).

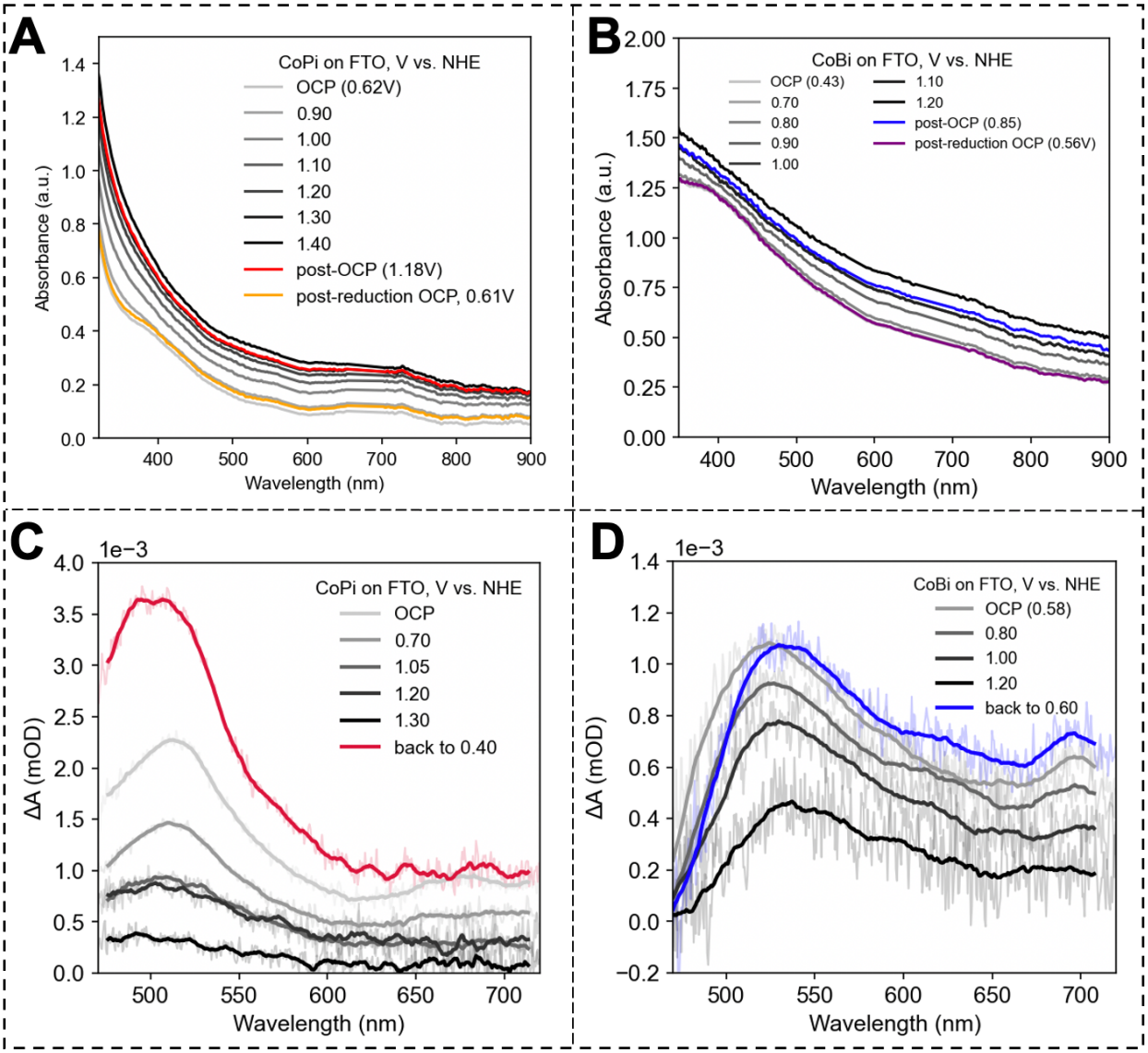

Figure 6. Steady state absorption spectra of (A) 96 mC/cm^2 CoPi and (B) 48 mC/cm^2 CoBi at varying applied potentials. Corresponding transient absorption spectral traces (time delay of 1.0 ns) of (C) 96 mC/cm^2 CoPi and (D) 48 mC/cm^2 CoBi are shown. For panels (C) and (D), a linear averaging function over 15 adjacent points was applied for visual separation of the spectral traces.

In order to gain further experimental insight into the origin of the observed spectroelectrochemical absorption changes, similar experiments were carried out in acetonitrile with 0.1 M $TBAPF_6$ supporting electrolyte. The same trends of increasing ground-state intensity and decreasing excited-state intensity were observed with increased oxidizing potential. No

substantial difference in absorption intensity changes were observed when titrating in buffered H_2O (**Figure S18**), despite an increase in current as apparent through cyclic voltammograms (**Figure S16**).

3. Discussion

3.1 Nature of photoexcited states in amorphous cobalt oxide films

Through the measurements described above, there are three complementary experimental observations to suggest that the long-lived photoexcited states in CoPi and CoBi films are attributable to trapped holes. These will be detailed below and consist of the following: 1) the increase in ground-state electronic absorption intensity with anodic bias, 2) the decrease of ESA intensity when excited with 380 nm light and monitored spectroelectrochemically under anodic bias, and 3) the quenching of decay kinetics in the presence of MeOH.

3.1.1 Ground-state absorption intensity increases under applied anodic bias

The ground-state absorption spectra of CoPi and CoBi exhibit higher intensity in the UV region. This spectral intensity can be attributed to ligand-to-metal charge transfer (LMCT) transitions, while the moderate intensity in the lower energy range can be attributed to ligand field (d-d) transitions and intervalence charge transfer (IVCT) bands. Similar band assignments have been made for Co_3O_4.[26] The broad rising absorption profile complicates the picture of a straightforward band structure as observed in many undoped crystalline metal oxides, in which the onset of absorbance appears clearly at the energy of the band gap.[27] The increasing ground-state absorption intensity with anodic bias is observed both in aqueous buffers and in acetonitrile with 0.1 M $TBAPF_6$ (**Figure 6**). The spectral shape in both the ground state and photoexcited states does not change appreciably in acetonitrile relative to native buffers (**Figure S31**). As would be expected for water oxidation, the current response is significantly less when oxidation occurs in acetonitrile as opposed to aqueous buffer (**Figure S16**). However, the non-negligible presence of faradaic current in acetonitrile suggests that oxidation events are taking place on the film, likely largely due to the conversion of Co(II) to Co(III). Similar behavior of the spectroelectrochemical difference spectrum in the UV-vis region of CoPi had been observed previously and attributed to increasing Co(III) character by Durrant and coworkers.[12]

3.1.2 The photoexcited state absorption intensity decreases under applied anodic bias

The ESA profile upon 380 nm excitation is similar to that of other metal oxides that host trapped hole or electron states upon photoexcitation. Similar UV-pumped excited-state spectra were observed for anatase TiO_2 nanoparticles (10 – 15 nm diameter)[28] and nitrogen-doped anatase TiO_2 powder.[29] In hematite, a µs – ms long-lived ESA band at 580 nm was attributed to hole absorption, whereas the long-lived ESA band in our study appears closer to 510 nm, with lifetimes in a comparable range (on the order of µs, with a generous stretching parameter in the case of stretched exponential fits as shown in **Table 1**).[30,31] The photoinduced holes in hematite were quenched by MeOH, as was observed in the case of CoPi and CoBi and detailed in the following section. Similar assignments in the visible probe region were made for several other systems, including 1) Cu_2O (transient absorption maxima at > 475 nm, quenched by Na_2SO_3),[32] 2) WO_3 (transient absorption maxima at 430 – 500 nm, quenched by methanol),[33–37] and 3) colloidal CdS (transient absorption maxima at 470 – 500 nm, quenched by NaI and thiophenol).[38–42] The use of exogenous electron donors and the resulting quenching effects supported the assignment of the transient absorption to photoinduced holes. The long-lived ESA observed here for CoPi and CoBi is, thus, consistent with photoinduced trapped holes.[43] As the film gets oxidized, the ground-state intensity increases from the increased number of holes in the form of Co(III) in the material. Consequently, the ESA intensity decreases as the trapped holes are filled with increasing applied potential, resulting in fewer holes to be generated by photoexcitation.

3.1.3 Photoexcited state decay kinetics are quenched in the presence of MeOH

When considering the band structure formalism, both the steady state and transient absorption spectra are consistent with the abundance of mid-gap states in amorphous cobalt oxide films. Similar to other metal oxides, such defect states can host either trapped holes or trapped electrons. To further characterize the nature of the trapped state, both electron and hole scavengers were added to monitor which quenches the excited state.[43] Both CoPi and CoBi excited states were found to be quenched in the presence of MeOH, a known hole scavenger (**Figure 5**).[43] A CoPi film was tested in the presence of H_2O, D_2O, phosphate buffer, MeOH (hole scavenger), 1.0 M Na_2SO_3 (electron scavenger), 1.0 M $AgNO_3$ (electron scavenger), and acetonitrile (**Figure S32**). Only MeOH resulted in a quenching effect, further suggesting the long-lived excited state is a

trapped hole state. A similar quenching effect in the presence of MeOH was observed in microcrystalline hematite films.[30]

3.2. Differences between the photoexcited spectra and the spectroelectrochemical difference spectra

As shown in **Figure 7**, the electrochemical difference spectra representing the additional intensity from injected holes under applied anodic bias and the transient absorption excited-state spectrum at long time intervals do not overlay or show much similarity, other than covering a broad region. The differences in the spectra observed in amorphous cobalt oxide upon photoexcitation versus electrochemical oxidation can be attributed to several factors rooted in the material's electronic structure and the nature of the excitation processes. Photoexcitation excites electrons across the bandgap, creating electron-hole pairs. The specific excitation energies involved can selectively populate certain trap states, leading to distinct spectral features. Electrochemical oxidation, on the other hand, alters the Fermi level leading to a broader range of accessible electronic transitions, including those involving defect states or surface states that are not directly accessed by photon absorption. The spectrum under pulsed laser excitation is influenced by the dynamics of electron-hole pairs and their interaction with intraband trap states.

Such differences were considered previously in microcrystalline hematite by Durrant and coworkers.[30] Under anodic bias, these trapped states become oxidized (electron-depleted), affecting how electrons and holes recombine and thus altering the spectral features. The lifetime of the photoexcited trapped holes was extended up the order of seconds under applied anodic bias, while the amplitude of the long-lived signal decreased.[30] In contrast to nanocrystalline hematite, amorphous materials typically have a more disordered structure than crystalline materials, leading to a higher density and different distribution of trap states. In CoPi and CoBi, we similarly observe a decrease in the amplitude of the excited-state signal upon application of anodic bias. We did not observe significant changes to the decay rate at a ps – ns timescale under applied anodic bias, though this does not rule out an effect on the μs – ms timescale. As such, it remains unclear whether there is a long-time component of the excited state decay that is sensitive to anodic bias. The trapped hole feature observed at ~510 nm for bandgap excitation of CoPi and CoBi suggests the presence of specific trap states that are effectively participating in hole trapping under photoexcitation conditions. Electrochemical oxidation of the ground state results in a broad,

featureless increase in intensity, indicating a more uniform distribution of trap states or a lack of specific spectral features associated with these states. In contrast to hematite, where specific trap states below the conduction band play a significant role, the behavior in CoPi and CoBi suggests a different mechanism or a more homogenous distribution of states within the bandgap. This is consistent with the disparities observed for the transient absorption spectra and spectroelectrochemical difference spectra profiles of CoPi and CoBi films.

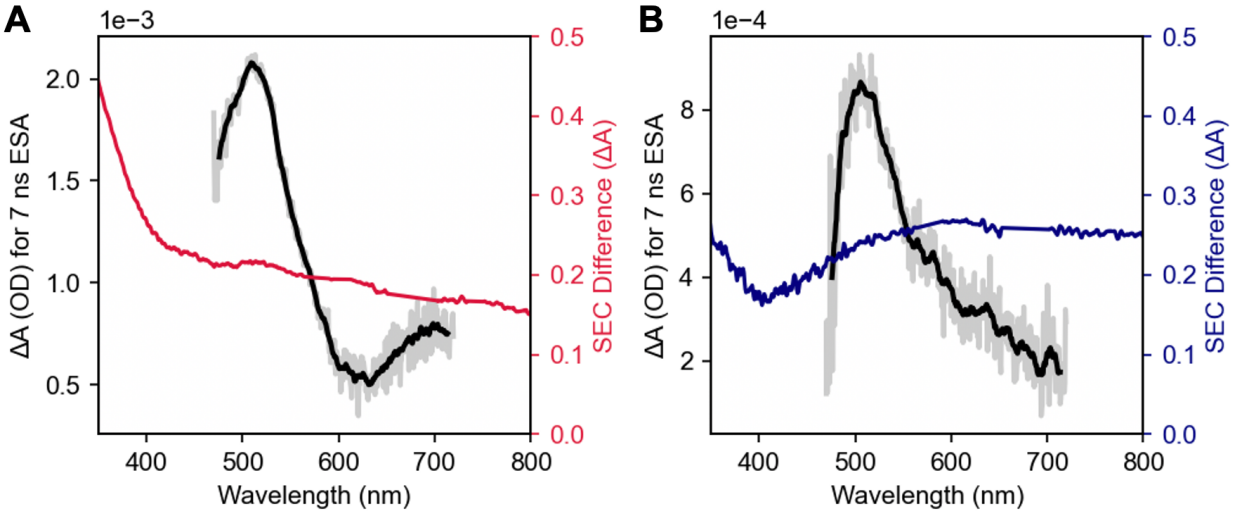

Figure 7. Comparisons between photoexcited ESA spectra with 7 ns pump-probe delay and the electrochemical difference spectra for CoPi **(A)** and CoBi (**B)** films in their respective buffered solutions. The spectroelectrochemical difference spectrum is the subtraction between the 1.4 V vs. NHE (OER overpotential of 0.58 V) spectrum and the open-circuit potential spectrum for CoPi, and the subtraction between 1.2 V vs. NHE (OER overpotential of 0.51 V) with the open-circuit potential spectrum for CoBi. Regions around 585 nm and 690 nm of the SEC difference spectrum have been omitted and replaced with a connecting straight line as the spectrometer lamp exhibited saturating artifacts at those wavelengths.

3.3 Implications of long-lived excited states for the oxygen evolution reaction (OER)

The excited-state spectral shapes and decay kinetics of CoPi and CoBi films were not significantly affected by solvent conditions, except for MeOH (**Figure S32**). This suggests that the long-lived excited states would more likely correspond to deep traps in the middle of the band gap, rather than shallow traps, which would be shorter-lived and more sensitive to external perturbations.[45] Furthermore, it has been postulated that deep hole trapping should be common to amorphous oxides and has been observed in materials such as a-SiO_2, a-Al_2O_3 and a-TiO_2.[46] Applied bias does not have a marked effect on any of the decay features (**Figure S19**). This is unlike observations for hematite photoanodes, where applied bias was found to have a significant retarding effect on

the electron-hole recombination rates.[44] Furthermore, the observation of similar change in absorption intensity upon applying anodic bias without the presence of H_2O suggests that H_2O itself is not necessary to stabilize the trap states. Therefore, there is nothing to suggest that the long-lived trapped hole states play a role in the OER. Nevertheless, the trapped hole states may still play a role in charge transport through the film and highlight the complicated electronic structural nature of the catalytic films. Future photoconductivity measurements may elucidate the potential role of these trapped states in charge transport.

3.4 Long-lived hole trap decay kinetics in CoPi and CoBi films

While the intermediate-range structure of the two films are known to differ, both the steady-state and time-resolved optical spectra of the films in the UV-vis do not show dramatic differences. Therefore, the differences in decay kinetics can be potentially tied to differences in the films' properties that would otherwise be undetectable from steady state methods. Due to the complicated electronic structure and amorphous nature of the materials, it is unsurprising that the kinetics of CoPi and CoBi films could not be fit to a simple multi-exponential model (**Figures S33, S34**). Instead, both CoPi and CoBi decays are best fit by a sum of two stretched exponentials of the form $\Delta A = a_1(e^{-k_1})^{\beta_1} + a_2(e^{-k_2})^{\beta_2}$. Stretched exponentials are commonly used to fit relaxation processes in disordered materials and semiconductor trap states, where the stretching term can be used as a metric for disorder within the films.[47–49] The fitted parameters are presented in **Table 1**. The low $\beta_1$and β_2 values may reflect the amorphous nature of the films. The long-lived excited-state decays of CoPi and CoBi are characterized here for the first time, with CoPi ultimately having a longer lifetime than CoBi despite CoPi having a much faster decay in the first 10 ps (**Figure 4**).

Table 1. Average fitted values for a phenomenological stretched biexponential model of decay.

	CoPi	CoBi
Normalized a_1 coefficient (%)	80%	29%
k_1	2.0×10^7 s^{-1}	1.9×10^6 s^{-1}
$\tau_1 = 1/k_1$	50 ns	0.5 µs
β_1	0.23	0.13
Normalized a_2 coefficient (%)	20%	71%
k_2	6.1×10^5 s^{-1}	1.7×10^6 s^{-1}
$\tau_2 = 1/k_2$	1.6 µs	0.6 µs
β_2	0.11	0.47

Conclusion

Dynamics from sub-picosecond to millisecond timescales were probed for the first time in CoPi and CoBi thin films using transient absorption spectroscopy, revealing structurally distinct photophysics and long-lived relaxation dynamics persisting beyond 10 ms. By applying spectroelectrochemistry in the ground- and photo-excited states, along with the observed excited-state quenching by a hole scavenger, these relaxation dynamics can be attributed to deep hole traps reminiscent of other metal oxides. Based on solvent-dependent transient absorption measurements, it is unclear whether the optically probed trap states are important for the OER. However, they could potentially play a role in charge transport and offer new electronic structural insights into the amorphous films.

Acknowledgements

RM acknowledges NSERC PGSD3-557779-2021 funding. Parts of this work were supported by NIH grant 1S10OD032151-01 for the purchase of a High-Energy Tunable Nanosecond-Pulsed Laser in the Beckman Institute Laser Resource Center. Financial support from Caltech and the Dow Next Generation Educator Fund is gratefully acknowledged.

References

(1) Service, R. F. Hydrogen Economy? Let Sunlight Do the Work. *Science* **2007**, *315* (5813), 789–789. https://doi.org/10.1126/science.315.5813.789.

(2) Barber, J. Photosynthetic Energy Conversion: Natural and Artificial. *Chem. Soc. Rev.* **2008**, *38* (1), 185–196. https://doi.org/10.1039/B802262N.

(3) Tachibana, Y.; Vayssieres, L.; Durrant, J. R. Artificial Photosynthesis for Solar Water-Splitting. *Nat. Photonics* **2012**, *6* (8), 511–518. https://doi.org/10.1038/nphoton.2012.175.

(4) Doyle, R. L.; Lyons, M. E. G. The Oxygen Evolution Reaction: Mechanistic Concepts and Catalyst Design. In *Photoelectrochemical Solar Fuel Production: From Basic Principles to Advanced Devices*; Giménez, S., Bisquert, J., Eds.; Springer International Publishing: Cham, 2016; pp 41–104. https://doi.org/10.1007/978-3-319-29641-8_2.

(5) Kanan, M. W.; Nocera, D. G. In Situ Formation of an Oxygen-Evolving Catalyst in Neutral Water Containing Phosphate and Co2+. *Science* **2008**, *321* (5892), 1072–1075. https://doi.org/10.1126/science.1162018.

(6) Surendranath, Y.; Kanan, M. W.; Nocera, D. G. Mechanistic Studies of the Oxygen Evolution Reaction by a Cobalt-Phosphate Catalyst at Neutral pH. *J. Am. Chem. Soc.* **2010**, *132* (46), 16501–16509. https://doi.org/10.1021/ja106102b.

(7) Nocera, D. G. The Artificial Leaf. *Acc. Chem. Res.* **2012**, *45* (5), 767–776. https://doi.org/10.1021/ar2003013.

(8) Reece, S. Y.; Hamel, J. A.; Sung, K.; Jarvi, T. D.; Esswein, A. J.; Pijpers, J. J. H.; Nocera, D. G. Wireless Solar Water Splitting Using Silicon-Based Semiconductors and Earth-Abundant Catalysts. *Science* **2011**, *334* (6056), 645–648. https://doi.org/10.1126/science.1209816.

(9) Khnayzer, R. S.; Mara, M. W.; Huang, J.; Shelby, M. L.; Chen, L. X.; Castellano, F. N. Structure and Activity of Photochemically Deposited "CoPi" Oxygen Evolving Catalyst on Titania. *ACS Catal.* **2012**, *2* (10), 2150–2160. https://doi.org/10.1021/cs3005192.

(10) Zhong, D. K.; Cornuz, M.; Sivula, K.; Grätzel, M.; Gamelin, D. R. Photo-Assisted Electrodeposition of Cobalt–Phosphate (Co–Pi) Catalyst on Hematite Photoanodes for Solar Water Oxidation. *Energy Environ. Sci.* **2011**, *4* (5), 1759–1764. https://doi.org/10.1039/C1EE01034D.

(11) Steinmiller, E. M. P.; Choi, K.-S. Photochemical Deposition of Cobalt-Based Oxygen Evolving Catalyst on a Semiconductor Photoanode for Solar Oxygen Production. *Proc. Natl. Acad. Sci.* **2009**, *106* (49), 20633–20636. https://doi.org/10.1073/pnas.0910203106.

(12) Ma, Y.; Kafizas, A.; Pendlebury, S. R.; Le Formal, F.; Durrant, J. R. Photoinduced Absorption Spectroscopy of CoPi on $BiVO_4$: The Function of CoPi during Water Oxidation. *Adv. Funct. Mater.* **2016**, *26* (27), 4951–4960. https://doi.org/10.1002/adfm.201600711.

(13) Jeon, T. H.; Choi, W.; Park, H. Cobalt–Phosphate Complexes Catalyze the Photoelectrochemical Water Oxidation of BiVO4 Electrodes. *Phys. Chem. Chem. Phys.* **2011**, *13* (48), 21392–21401. https://doi.org/10.1039/C1CP23135A.

(14) Zhang, J.; Jiang, D.; Wang, P.; Zhong, J.; Sun, G.; Yao, Y.; Luo, W.; Zou, Z. A High-Voltage Solar Rechargeable Device Based on a CoPi/$BiVO_4$ Faradaic Junction. *J. Mater. Chem. A* **2022**, *10* (4), 1802–1807. https://doi.org/10.1039/D1TA08949H.

(15) Sprague-Klein, E. A.; He, X.; Mara, M. W.; Reinhart, B. J.; Lee, S.; Utschig, L. M.; Mulfort, K. L.; Chen, L. X.; Tiede, D. M. Photo-Electrochemical Effect in the Amorphous

Cobalt Oxide Water Oxidation Catalyst Cobalt–Phosphate (CoPi). *ACS Energy Lett.* **2022**, *7* (9), 3129–3138. https://doi.org/10.1021/acsenergylett.2c01560.
(16) Ullman, A. M.; Brodsky, C. N.; Li, N.; Zheng, S.-L.; Nocera, D. G. Probing Edge Site Reactivity of Oxidic Cobalt Water Oxidation Catalysts. *J. Am. Chem. Soc.* **2016**, *138* (12), 4229–4236. https://doi.org/10.1021/jacs.6b00762.
(17) Hadt, R. G.; Hayes, D.; Brodsky, C. N.; Ullman, A. M.; Casa, D. M.; Upton, M. H.; Nocera, D. G.; Chen, L. X. X-Ray Spectroscopic Characterization of Co(IV) and Metal–Metal Interactions in Co_4O_4: Electronic Structure Contributions to the Formation of High-Valent States Relevant to the Oxygen Evolution Reaction. *J. Am. Chem. Soc.* **2016**, *138* (34), 11017–11030. https://doi.org/10.1021/jacs.6b04663.
(18) Brodsky, C. N.; Hadt, R. G.; Hayes, D.; Reinhart, B. J.; Li, N.; Chen, L. X.; Nocera, D. G. In Situ Characterization of Cofacial Co(IV) Centers in Co_4O_4 Cubane: Modeling the High-Valent Active Site in Oxygen-Evolving Catalysts. *Proc. Natl. Acad. Sci.* **2017**, *114* (15), 3855–3860. https://doi.org/10.1073/pnas.1701816114.
(19) Kanan, M. W.; Yano, J.; Surendranath, Y.; Dincă, M.; Yachandra, V. K.; Nocera, D. G. Structure and Valency of a Cobalt−Phosphate Water Oxidation Catalyst Determined by in Situ X-Ray Spectroscopy. *J. Am. Chem. Soc.* **2010**, *132* (39), 13692–13701. https://doi.org/10.1021/ja1023767.
(20) Surendranath, Y.; Lutterman, D. A.; Liu, Y.; Nocera, D. G. Nucleation, Growth, and Repair of a Cobalt-Based Oxygen Evolving Catalyst. *J. Am. Chem. Soc.* **2012**, *134* (14), 6326–6336. https://doi.org/10.1021/ja3000084.
(21) Brodsky, C. N.; Bediako, D. K.; Shi, C.; Keane, T. P.; Costentin, C.; Billinge, S. J. L.; Nocera, D. G. Proton–Electron Conductivity in Thin Films of a Cobalt–Oxygen Evolving Catalyst. *ACS Appl. Energy Mater.* **2019**, *2* (1), 3–12. https://doi.org/10.1021/acsaem.8b00785.
(22) Farrow, C. L.; Bediako, D. K.; Surendranath, Y.; Nocera, D. G.; Billinge, S. J. L. Intermediate-Range Structure of Self-Assembled Cobalt-Based Oxygen-Evolving Catalyst. *J. Am. Chem. Soc.* **2013**, *135* (17), 6403–6406. https://doi.org/10.1021/ja401276f.
(23) Risch, M.; Khare, V.; Zaharieva, I.; Gerencser, L.; Chernev, P.; Dau, H. Cobalt−Oxo Core of a Water-Oxidizing Catalyst Film. *J. Am. Chem. Soc.* **2009**, *131* (20), 6936–6937. https://doi.org/10.1021/ja902121f.
(24) Risch, M.; Klingan, K.; Ringleb, F.; Chernev, P.; Zaharieva, I.; Fischer, A.; Dau, H. Water Oxidation by Electrodeposited Cobalt Oxides—Role of Anions and Redox-Inert Cations in Structure and Function of the Amorphous Catalyst. *ChemSusChem* **2012**, *5* (3), 542–549. https://doi.org/10.1002/cssc.201100574.
(25) Kwon, G.; Jang, H.; Lee, J.-S.; Mane, A.; Mandia, D. J.; Soltau, S. R.; Utschig, L. M.; Martinson, A. B. F.; Tiede, D. M.; Kim, H.; Kim, J. Resolution of Electronic and Structural Factors Underlying Oxygen-Evolving Performance in Amorphous Cobalt Oxide Catalysts. *J. Am. Chem. Soc.* **2018**, *140* (34), 10710–10720. https://doi.org/10.1021/jacs.8b02719.
(26) Qiao, L.; Xiao, H. Y.; Meyer, H. M.; Sun, J. N.; Rouleau, C. M.; Puretzky, A. A.; Geohegan, D. B.; Ivanov, I. N.; Yoon, M.; Weber, W. J.; Biegalski, M. D. Nature of the Band Gap and Origin of the Electro-/Photo-Activity of Co_3O_4. *J. Mater. Chem. C* **2013**, *1* (31), 4628–4633. https://doi.org/10.1039/C3TC30861H.
(27) Makuła, P.; Pacia, M.; Macyk, W. How To Correctly Determine the Band Gap Energy of Modified Semiconductor Photocatalysts Based on UV–Vis Spectra. *J. Phys. Chem. Lett.* **2018**, *9* (23), 6814–6817. https://doi.org/10.1021/acs.jpclett.8b02892.

(28) Yoshihara, T.; Katoh, R.; Furube, A.; Tamaki, Y.; Murai, M.; Hara, K.; Murata, S.; Arakawa, H.; Tachiya, M. Identification of Reactive Species in Photoexcited Nanocrystalline TiO_2 Films by Wide-Wavelength-Range (400−2500 Nm) Transient Absorption Spectroscopy. *J. Phys. Chem. B* **2004**, *108* (12), 3817–3823. https://doi.org/10.1021/jp031305d.
(29) Yamanaka, K.; Morikawa, T. Charge-Carrier Dynamics in Nitrogen-Doped TiO_2 Powder Studied by Femtosecond Time-Resolved Diffuse Reflectance Spectroscopy. *J. Phys. Chem. C* **2012**, *116* (1), 1286–1292. https://doi.org/10.1021/jp209210u.
(30) Pendlebury, S. R.; Barroso, M.; Cowan, A. J.; Sivula, K.; Tang, J.; Grätzel, M.; Klug, D.; Durrant, J. R. Dynamics of Photogenerated Holes in Nanocrystalline α-Fe_2O_3 Electrodes for Water Oxidation Probed by Transient Absorption Spectroscopy. *Chem. Commun.* **2010**, *47* (2), 716–718. https://doi.org/10.1039/C0CC03627G.
(31) Huang, Z.; Lin, Y.; Xiang, X.; Rodríguez-Córdoba, W.; McDonald, K. J.; Hagen, K. S.; Choi, K.-S.; Brunschwig, B. S.; Musaev, D. G.; Hill, C. L.; Wang, D.; Lian, T. In Situ Probe of Photocarrier Dynamics in Water-Splitting Hematite (α-Fe_2O_3) Electrodes. *Energy Environ. Sci.* **2012**, *5* (10), 8923–8926. https://doi.org/10.1039/C2EE22681B.
(32) Pastor, E.; Pesci, F. M.; Reynal, A.; Handoko, A. D.; Guo, M.; An, X.; Cowan, A. J.; Klug, D. R.; Durrant, J. R.; Tang, J. Interfacial Charge Separation in Cu_2O/RuOx as a Visible Light Driven CO_2 Reduction Catalyst. *Phys. Chem. Chem. Phys.* **2014**, *16* (13), 5922–5926. https://doi.org/10.1039/C4CP00102H.
(33) Cristino, V.; Marinello, S.; Molinari, A.; Caramori, S.; Carli, S.; Boaretto, R.; Argazzi, R.; Meda, L.; Bignozzi, C. A. Some Aspects of the Charge Transfer Dynamics in Nanostructured WO_3 Films. *J. Mater. Chem. A* **2016**, *4* (8), 2995–3006. https://doi.org/10.1039/C5TA06887H.
(34) Kim, W.; Tachikawa, T.; Monllor-Satoca, D.; Kim, H.; Majima, T.; Choi, W. Promoting Water Photooxidation on Transparent WO_3 Thin Films Using an Alumina Overlayer. *Energy Environ. Sci.* **2013**, *6* (12), 3732–3739. https://doi.org/10.1039/C3EE42151A.
(35) Zhai, X.-P.; Gao, L.-F.; Zhang, H.; Peng, Y.; Zhang, X.-D.; Wang, Q.; Zhang, H.-L. Defect Engineering of Ultrathin WO_3 Nanosheets: Implications for Nonlinear Optoelectronic Devices. *ACS Appl. Nano Mater.* **2022**, *5* (1), 1169–1177. https://doi.org/10.1021/acsanm.1c03791.
(36) Sachs, M.; Park, J.-S.; Pastor, E.; Kafizas, A.; Wilson, A. A.; Francàs, L.; Gul, S.; Ling, M.; Blackman, C.; Yano, J.; Walsh, A.; Durrant, J. R. Effect of Oxygen Deficiency on the Excited State Kinetics of WO_3 and Implications for Photocatalysis. *Chem. Sci.* **2019**, *10* (22), 5667–5677. https://doi.org/10.1039/C9SC00693A.
(37) Pesci, F. M.; Cowan, A. J.; Alexander, B. D.; Durrant, J. R.; Klug, D. R. Charge Carrier Dynamics on Mesoporous WO_3 during Water Splitting. *J. Phys. Chem. Lett.* **2011**, *2* (15), 1900–1903. https://doi.org/10.1021/jz200839n.
(38) Kamat, P. V.; Dimitrijevic, N. M.; Fessenden, R. W. Photoelectrochemistry in Particulate Systems. 6. Electron-Transfer Reactions of Small Cadmium Sulfide Colloids in Acetonitrile. *J. Phys. Chem.* **1987**, *91* (2), 396–401. https://doi.org/10.1021/j100286a029.
(39) Kamat, P. V.; Ebbesen, T. W.; Dimitrijević, N. M.; Nozik, A. J. Primary Photochemical Events in CdS Semiconductor Colloids as Probed by Picosecond Laser Flash Photolysis. *Chem. Phys. Lett.* **1989**, *157* (5), 384–389. https://doi.org/10.1016/0009-2614(89)87267-7.

(40) Uchihara, T.; Fox, M. A. Nanosecond Laser Flash Photolysis of Thiophenolate-Capped Cadmium Sulfide Particles in Acetonitrile. *Inorganica Chim. Acta* **1996**, *242* (1), 253–259. https://doi.org/10.1016/0020-1693(96)04875-X.
(41) Uchihara, T.; Oshiro, H.; Kinjo, A. Subpicosecond Studies of Primary Photochemical Events of CdS Particles with Surface Modified by Various Capping Agents. *J. Photochem. Photobiol. Chem.* **1998**, *114* (3), 227–234. https://doi.org/10.1016/S1010-6030(98)00225-1.
(42) Wang, W.; Tao, Y.; Fan, J.; Yan, Z.; Shang, H.; Phillips, D. L.; Chen, M.; Li, G. Fullerene–Graphene Acceptor Drives Ultrafast Carrier Dynamics for Sustainable CdS Photocatalytic Hydrogen Evolution. *Adv. Funct. Mater.* **2022**, *32* (23), 2201357. https://doi.org/10.1002/adfm.202201357.
(43) Schneider, J.; Curti, M. Spectroscopic and Kinetic Characterization of Photogenerated Charge Carriers in Photocatalysts. *Photochem. Photobiol. Sci.* **2022**. https://doi.org/10.1007/s43630-022-00297-x.
(44) Pendlebury, S. R.; Wang, X.; Le Formal, F.; Cornuz, M.; Kafizas, A.; Tilley, S. D.; Grätzel, M.; Durrant, J. R. Ultrafast Charge Carrier Recombination and Trapping in Hematite Photoanodes under Applied Bias. *J. Am. Chem. Soc.* **2014**, *136* (28), 9854–9857. https://doi.org/10.1021/ja504473e.
(45) Viswanath, A. K. Chapter 3 - Surface and Interfacial Recombination in Semiconductors. In *Handbook of Surfaces and Interfaces of Materials*; Nalwa, H. S., Ed.; Academic Press: Burlington, 2001; pp 217–284. https://doi.org/10.1016/B978-012513910-6/50010-4.
(46) Strand, J.; Kaviani, M.; Gao, D.; El-Sayed, A.-M.; Afanas'ev, V. V.; Shluger, A. L. Intrinsic Charge Trapping in Amorphous Oxide Films: Status and Challenges. *J. Phys. Condens. Matter* **2018**, *30* (23), 233001. https://doi.org/10.1088/1361-648X/aac005.
(47) Zatryb, G.; Podhorodecki, A.; Misiewicz, J.; Cardin, J.; Gourbilleau, F. On the Nature of the Stretched Exponential Photoluminescence Decay for Silicon Nanocrystals. *Nanoscale Res. Lett.* **2011**, *6* (1), 106. https://doi.org/10.1186/1556-276X-6-106.
(48) Van de Walle, C. G. Stretched-Exponential Relaxation Modeled without Invoking Statistical Distributions. *Phys. Rev. B* **1996**, *53* (17), 11292–11295. https://doi.org/10.1103/PhysRevB.53.11292.
(49) Cui, B.; Milkus, R.; Zaccone, A. The Relation between Stretched-Exponential Relaxation and the Vibrational Density of States in Glassy Disordered Systems. *Phys. Lett. A* **2017**, *381* (5), 446–451. https://doi.org/10.1016/j.physleta.2016.12.003.

For Table of Contents Only